## COMMUNICATION

# Highly reversible lithium storage in a 3D macroporous Ge@C composite

Jianxiu Cheng, Jiaqing Wang, Weihan Li, Xiaowu Liu and Yan Yu*

A porous Ge@C composite was synthesized by magnesiothermic reduction reaction of $GeO_2$, Mg powder and glucose followed by an etching process with HCl solution. Compared to a porous Ge electrode, the porous Ge@C composite electrode delivers better cycling stability ($\sim$100% capacity retention after 100 cycles at the 0.2 C rate) and higher rate capability (440 mA h $g^{-1}$ at 1800 mA $g^{-1}$). The improved electrochemical performance results from the synergistic effect of the 3D interconnected porous structure and the carbon shells. The local pores could buffer the volume change and the conductive carbon shell could prevent the aggregation of Ge as well as enhance the electronic conductivity of the whole electrode.

## 1. Introduction

Lithium-ion batteries (LIBs) are among the most promising energy storage devices for electric vehicles (EVs) owing to their high power and energy.[1–3] For commercialization of EVs, the electrochemical performance and safety of LIBs still need further improvement, and thus it is essential to develop electrode materials with higher reversible capacity.[4–6] Compared with the traditional graphite anode, which has a theoretical specific capacity of 372 mA h $g^{-1}$, group IV A materials such as Si, Ge and Sn have been considered as very promising anode materials for LIBs because of their higher theoretical specific capacities (4200 mA h $g^{-1}$ for Si, 1600 mA h $g^{-1}$ for Ge, and 991 mA h $g^{-1}$ for Sn).[7–9] Among these, Ge has attracted much attention because of its excellent lithium-ion diffusivity (400 times faster than in Si), high electrical conductivity ($\sim$100 times higher than Si), and higher theoretical specific capacity.[10–14] However, the practical application of Ge anode has thus been mainly prevented by the enormous volume change (300–400%) experienced during the lithiation/delithiation process, which results in more capacity losses due to increased solid electrolyte interphase (SEI) formation while delamination results in loss of electrical contact with the current collector.[12,15] To mitigate the above-mentioned challenges and improve the cyclability of Ge anode, much effort has been made to minimize such volume strain during Li–Ge alloying/dealloying process, including the use of 0D nanoparticles, 1D nanowires, hollow nanotube, and 3D-porous nanoparticles.[10,12,16–26] Another effective approach to improve the capacity retention is to construct Ge–carbon composites (such as Ge nanoparticles on CNT and Ge–C core–shell).[27,28] Among those morphologies, 3D porous structure with conductive carbon coating has been proven to be most effective in accommodating the volume changes of electrode materials during cycling, because the local void space can buffer the volume change and the carbon coating can prevent the aggregation of active material. For instance, Cho *et al.* synthesized 3D porous Ge using a template method, which induces a very stable cycling performance (1400 mA h $g^{-1}$ at a rate of 1 C), showing only a 2% capacity decrease after 100 cycles.[17]

Taking advantages offered by both porous nanostructure and conductive carbon coating on the electrode materials, we herein report a carbon coated 3D macroporous Ge (denoted as porous Ge@C) anode material using a facile magnesiothermic reduction reaction of $GeO_2$, Mg and glucose under $Ar/H_2$ atmosphere in an open crucible.[29,30] To demonstrate the improvement of electrochemical performance of 3D porous Ge@C, we also prepared porous Ge and carbon coated Ge particles (denoted as Ge@C) as anode materials for LIBs, respectively. The obtained porous Ge@C composite shows the best electrochemical performance and delivers 776 mA h $g^{-1}$ after 100 cycles at 0.2 C. When cycled at a current density of 1800 mA $g^{-1}$, it still displays a reversible capacity as high as $\sim$500 mA h $g^{-1}$. This specific 3D porous structure plays an important role in optimizing electrochemical performance of the Ge anode. Firstly, the 3D porous structure offers enough void space to buffer the volume change and prevent electronic isolation after long life cycle; secondly, the uniform surface

*CAS Key Laboratory of Materials for Energy Conversion, Department of Materials Science and Engineering, University of Science and Technology of China, Hefei 230026, Anhui, P. R. China. E-mail: yanyumse@ustc.edu.cn*

conductive carbon coating provides electron percolation paths from the current collector to the active particles (3D porous Ge); thirdly, the carbon coating layer could effective prevent the aggregation of Ge during alloying/dealloying process.

## 2.   Experimental

### 2.1   Synthesis of porous Ge@C composite, Ge@C composite and porous Ge

The porous Ge@C composite was synthesized by a facile magnesiothermic reduction reaction under Ar/H$_2$ atmosphere. In a typical procedure, 0.3 g germanium dioxide (99.9%, Sigma Aldrich), 0.2 g Mg power (99%, Sigma Aldrich, −325 mesh) and 0.25 g glucose (99.9%, Sigma Aldrich) were mixed completely and ground to get a uniform gray mixture in the glove box filled with Ar. The obtained mixture then was heated in a tube furnace at 650 °C for 4 h under Ar (95 v%)/H$_2$ (5 v%) atmosphere. The heating rate was kept at 3 °C min$^{-1}$. The obtained black power was immersed by 1 M HCl solution and ultrasound one hour to remove MgO. Then the powder was washed with ethanol and dried at 70 °C in a vacuum oven for 12 h. For comparison, 0.3 g germanium dioxide and 0.2 g Mg powder were mixed and ground, then the gray powder was heated at 650 °C to get pure porous Ge powder. Germanium dioxide and glucose were ground and then were heated to get Ge@C composite.

### 2.2   Characterization techniques

The structure and morphology of the obtained samples was characterized by X-ray diffraction (XRD, Philips X'Pert Pro Cu K$_\alpha$ radiation), field-emission scanning electron microscopy (FESEM, JEOL, Tokyo, Japan) and high-resolution transmission electron microscopy (HETEM, JEOL 4000EX Tokyo, Japan). The thermogravimetric differential thermal analysis of porous Ge@C power was conducted with a thermogravimetry differential thermal analyzer (Shi-madzu, TGA-50) under air atmosphere with a heating rate of 10 °C min$^{-1}$ from room temperature to 1000 °C.

### 2.3   Electrochemical measurements

Electrochemical measurements were performed using CR2032 coin-type cells assembled in glove box filled with Ar. The active material, (porous Ge@C composite, Ge@C composite or porous Ge powers) carbon black and PVDF were mixed in a mass ratio of 75 : 15 : 10. The resultant slurry was then uniformly coated on a Cu foil current collector and dried at 80 °C in vacuum oven. Electrochemical cells were assembled with porous Ge@C composite, Ge@C composite or porous Ge electrode, metallic lithium foil as counter electrode and Celgard 2400 as separator. The weight of each piece of electrode is around 2 mg. The electrolyte was a solution of 1 M LiPF$_6$ in ethylene carbonate and diethyl carbonate (EC : DEC = 1 : 1, v/v). The cells were charged and discharged galvanostatically in the fixed voltage window from 5 mV to 1.5 V on a Neware battery tester at room temperature.

## 3.   Results and discussion

Fig. 1a shows the XRD patterns of the porous Ge@C composite, Ge@C composite and porous Ge, in which all peaks are in agreement with pure Ge (JCPDS card no. 04-0545). No GeO$_2$ or MgO peaks were detected, indicating the impurity phases were totally removed after washing with HCl. The absence peak of carbon in the XRD patterns of porous Ge@C composite implies that the carbon is not well crystallized. The (002) peak of porous Ge@C at 27.3° that is very close to (002) peak of graphite (27°), which may be attribute to a more graphitic carbon coating layer formation after heating in Ar/H$_2$ atmosphere. Fig. 1b presents the TGA-DSC profiles of the porous Ge@C, performed inflowing
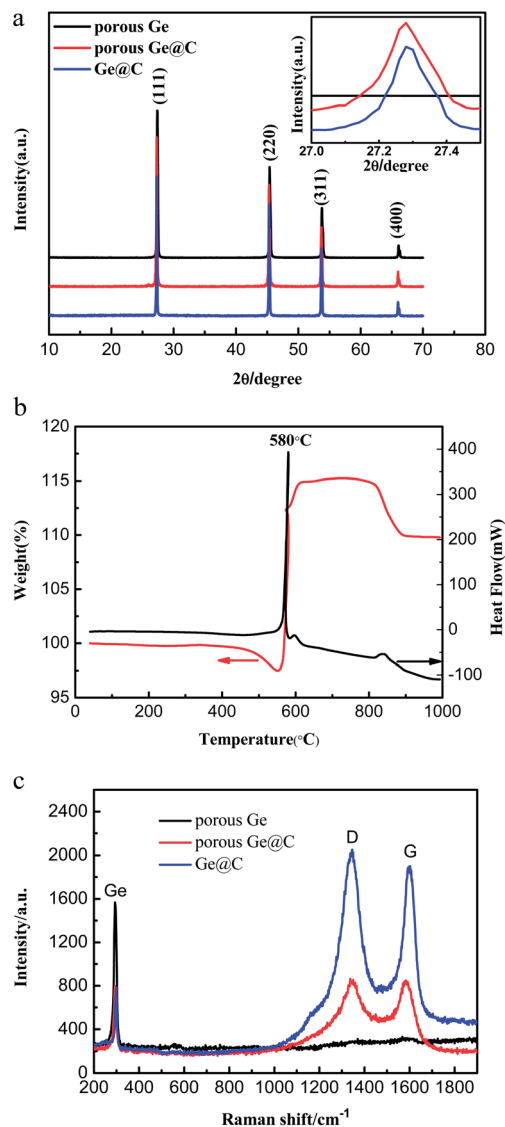


Fig. 1   (a) XRD patterns of porous Ge, porous Ge@C composite and Ge@C composite. The peak positions and intensities for cubic phase Ge are marked in the XRD (JCPDS no. 04-0545). The inset image is the magnified XRD patterns of porous Ge@C composite and Ge@C composite from 27° to 27.5°. (b) TGA-DSC curves of porous Ge@C composite. Heat rate is 10 °C min$^{-1}$. (c) Raman spectra of porous Ge, porous Ge@C composite and Ge@C composite.

air with a heating rate of 10 °C min$^{-1}$. A sharp exothermic peak of DSC curve centered at 580 °C is observed, which corresponds to the oxidation of Ge to GeO$_2$. The weight loss at around 800 °C is caused by carbon combustion reaction. TGA curve shows that the carbon and Ge weight contents are approximate 23 wt% and 77 wt%, respectively. The TGA-DSC profiles of Ge@C composite have the same result. Further structural information is provided by the Raman spectra in Fig. 1c. Appearance of a strong Raman peak located at 298 cm$^{-1}$ in porous Ge confirms the well crystalline Ge. In case of porous Ge@C composite and Ge@C composite, the intensity of Ge declines and the D and G band of carbon appears which proves that carbon has a certain proportion in composite. The ordering of carbon in the composite can also be seen in Raman spectra. The intensity ratio of the D band to the G band is 1.02 : 1 in porous Ge@C composite (red line) and 1.08 : 1 in Ge@C composite (blue line), which also indicated the formation of a disordered carbon structure. In case of Ge@C composite, the degree of disordering of carbon is higher than that of porous Ge@C composite.

SEM images (Fig. 2) reveal the structure of porous Ge, porous Ge@C composite and Ge@C composite synthesized by GeO$_2$ and glucose. The particles of porous Ge (Fig. 2a), with a size of around 5 μm, exhibit a coherent macroscopic network structure with a pore size distribution ranging from 200 nm to 600 nm in diameter. Fig. 2b shows the wall thickness of pores ranges from 150 to 250 nm. When the precursor materials contain glucose, the obtained porous Ge@C composite (Fig. 2c) displays similar porous structure with the pure porous Ge powder. The pore size decreases to 100–200 nm, which attributes to the carbon partially filled in the interconnecting macropores of Ge and conform coated on the Ge surface. When GeO$_2$ was reacted directly with glucose, the product presents block structure (Fig. 2e and f) and the shape of particles is extremely irregular. This proves that the appearance of pores in porous Ge@C composite is due to the participation of magnesium powder.

The 3D interconnected porous structure of the Ge@C composite and Ge powder are further confirmed by the transmission electron microscopy (TEM) micrograph (Fig. 3a and c). The high-resolution transmission electron microscopy (HRTEM) (Fig. 3b) reveals that the porous Ge powder have a diamond cubic structure. After coated with carbon, the Ge remains the cubic structure, where crystalline planes of Ge (220) with a distance spacing of 0.2 nm can be clearly observed. It can also clearly be seen that the porous Ge are well-covered by a carbon layer with a thickness of 4 nm (Fig. 3d). For Ge@C composite (Fig. 3e and f), the distribution of Ge and C is not uniform compared with the porous Ge@C composite. Furthermore, the distance of the crystalline planes of Ge becomes larger.
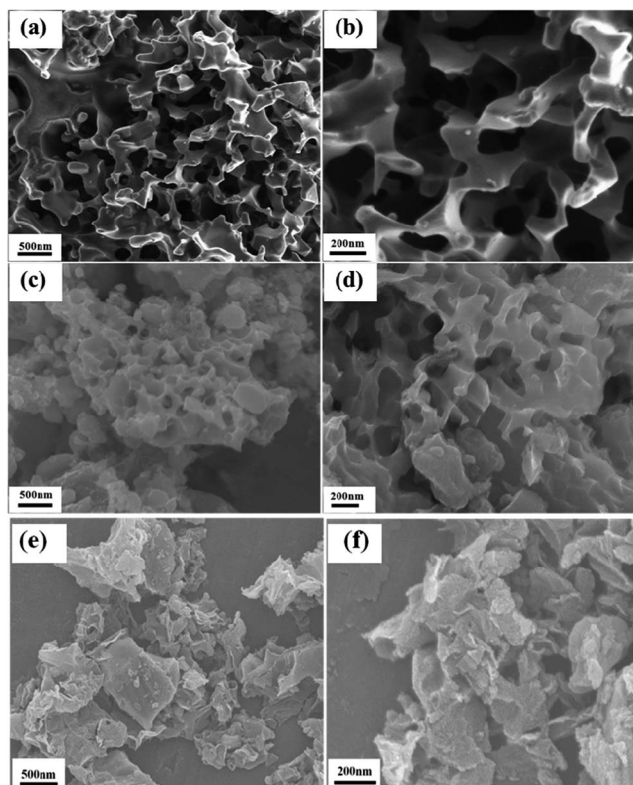


**Fig. 2** SEM image (a) and FESEM image (b) of porous Ge. SEM image (c) and FESEM image (d) of porous Ge@C composite. SEM image (e) and (f) of Ge@C composite.
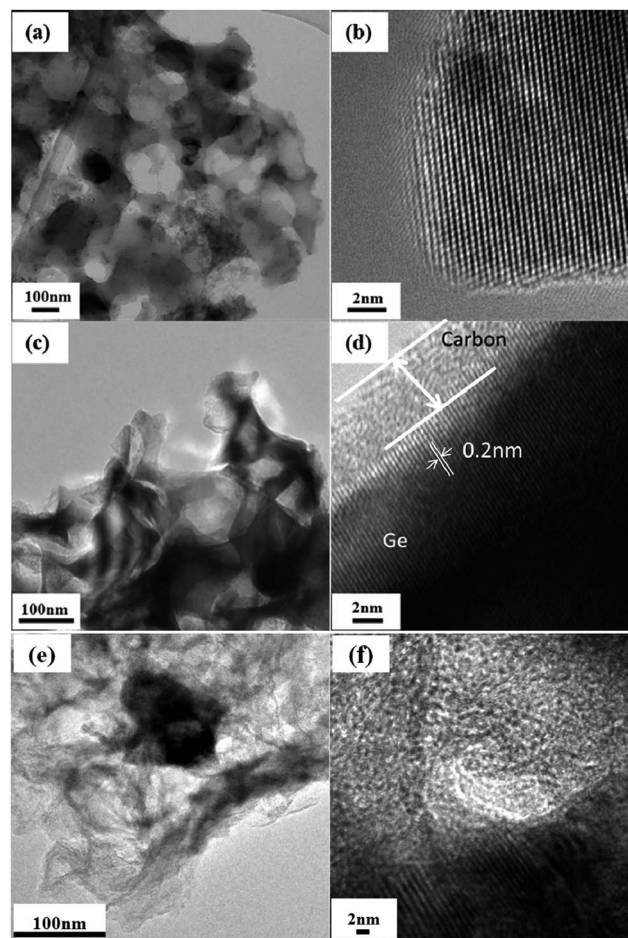


**Fig. 3** TEM image (a) and HRTEM image (b) of porous Ge. TEM image (c) and HRTEM image (d) of porous Ge@C composite. TEM image (e) and HRTEM image (f) of Ge@C composite.

Fig. 4a–c display the galvanostatic discharge–charge voltage profiles and cycling performance of porous Ge, porous Ge@C composite and Ge@C composite at 0.2 C (320 mA g$^{-1}$) in the voltage range of 0.005–1.5 V, respectively. Two plateaus (Fig. 4a) were observed at 0.2 V and 0.4 V during the first discharge process, which can be related to the alloying of Li with Ge.[32] The first discharge and charge capacities are 1738 and 1073 mA h g$^{-1}$ for the porous Ge powder, with an initial Coulombic efficiency (CE) of 61%. The large capacity loss is most likely attributed to formation of SEI layer on the electrode surface during the first discharge step.[31,32] In case of porous Ge@C composite (Fig. 4b), it delivers a capacity of 1821 and 981 mA h g$^{-1}$ for 1$^{st}$ discharge and charge, respectively, corresponding an initial CE of 53.9%. The higher initial capacity loss of porous Ge@C composite than that of Ge powder may result from enhanced formation of SEI layers on the porous Ge@C composite surface during the first cycles.[33,34] After the first cycle, the CE of porous Ge@C composite electrode was significantly improved to 99% for up to 100 cycles. For Ge@C composite

(Fig. 4c), it shows a capacity of 1763 and 852 mA h g$^{-1}$ for the first discharge and charge, respectively, with an initial CE of 48.3%. In the following cycles, the capacity decreased rapidly, indicting lower capacity retention of Ge@C composite.

Fig. 4d shows the capacity retention of porous Ge, porous Ge@C composite and Ge@C composite electrodes at 0.2 C. The capacity of Ge@C composite decreases rapidly after two cycles because that there are no pores to sustain the large volume change during discharge and charge processes. Both porous Ge and porous Ge@C composite powder delivers similar capacity in the first 20 cycles. The capacity of porous Ge powder degrades rapidly afterwards result from the large volume change (>300%) during lithium alloying/dealloying processes, leading to an electrical disconnection between particles. In contrast, porous Ge@C composite electrode shows a significantly improved cyclability. It could be attributed to the special carbon coated porous structure, which confined a variety of advantages: offering sufficient void space to accommodate the large volume change, providing an interconnected electron and ion transfer
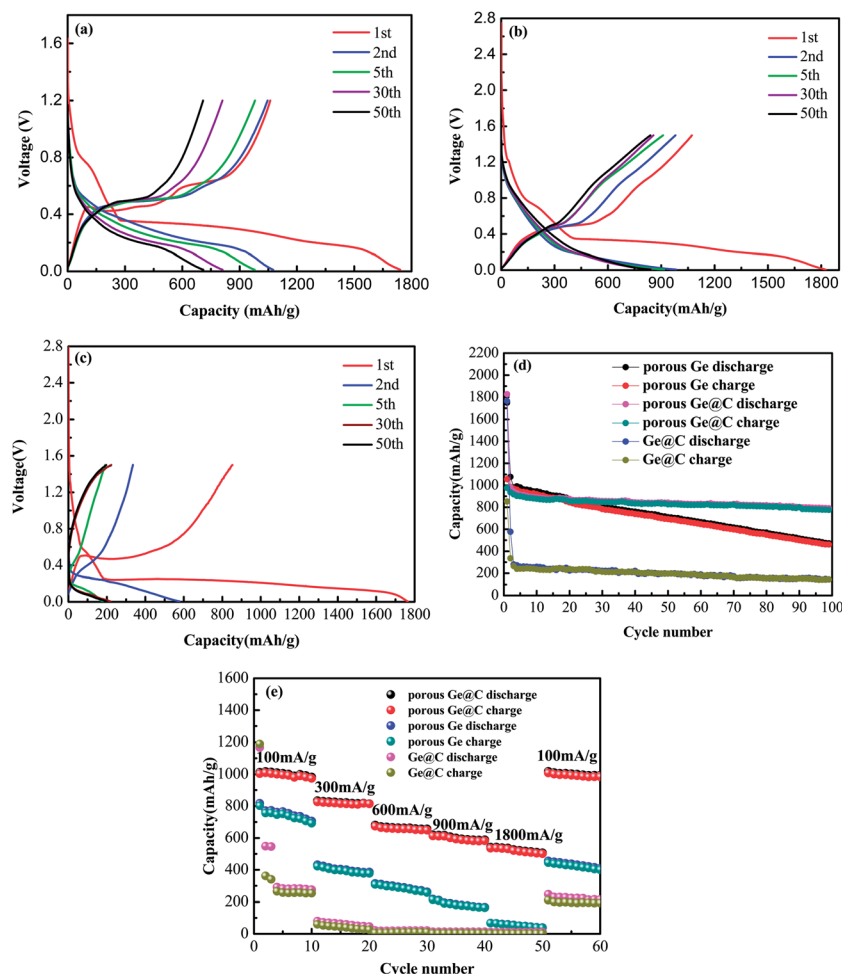


**Fig. 4** Electrochemical performance of porous Ge, porous Ge@C composite and Ge@C composite electrodes cycled between 0.005 V and 1.5 V vs. Li$^+$/Li. Voltage profiles of the porous Ge electrode (a), porous Ge@C composite electrode (b) and Ge@C composite electrode (c) at a cycling rate of 0.2 C, the cycle numbers were marked in the picture; (d) capacity retention of porous Ge, porous Ge@C composite and Ge@C composite electrodes at 0.2 C rate. (e) Rate capability of porous Ge, porous Ge@C composite and Ge@C composite electrodes. (The current density was marked in the picture.)

path during the long cycle life, preventing cracking as well as morphology stability. The porous Ge@C composite electrode still delivers a reversible capacity of ~790 mA h g$^{-1}$ after 100 cycles at 0.2 C, which is ~2 times higher than that of the theoretical capacity of graphite. Furthermore, as shown in Fig. 4e, the porous Ge@C composite electrode also shows a better rate capability than porous Ge electrode and Ge@C composite at the same current density. The porous Ge@C composite electrode delivers reversible capacities of 590, 530, and 440 mA h g$^{-1}$ at 600, 900, and 1800 mA g$^{-1}$, respectively. Note that after cycled at high C rate, the electrode can recover and delivers a reversible capacity as high as 1015 mA h g$^{-1}$ when the current density was tuned back to 100 mA g$^{-1}$, implying its good reversibility. In case of porous Ge electrode, it only delivers capacities of 300, 180, and 50 mA h g$^{-1}$ at the same current density. And for Ge@C composite, it only displays reversible capacities of 20, 12, and 11 mA h g$^{-1}$ at the same current density, respectively.

Notably, the discharge capacity of both porous Ge@C and porous Ge at higher current density (320 mA g$^{-1}$ in Fig. 4c) are better than those obtained from the stepwise cycling starting from 100 mA g$^{-1}$ (Fig. 4e). It could be attributed to the interfacial storage of lithium, which has been demonstrated in mesoporous TiO$_2$ anode.[35]

# 4. Conclusions

In conclusion, we have successfully fabricated porous Ge@C composite *via* magnesiothermic reduction reaction of GeO$_2$, Mg and glucose. The porous Ge@C composite exhibits a coherent macroscopic network structure with a pore size distribution ranging from 200 nm to 600 nm in diameter and a uniform carbon coated layer (~4 nm) on the surface. As an anode material for LIBs, the porous Ge@C composite exhibits excellent cycling performance and improved rate capability in comparison with porous Ge electrode, which attributes to the synergistic effect of 3D interconnected porous structure and conducting carbon shell. The local pore could buffer the volume change and the conductive carbon shell could prevent the aggregation of Ge as well as enhance the electronic conductivity of the whole electrode. This porous Ge@C composite can be considered as a promising anode material for LIBs.

## Acknowledgements

## References

1 L. Ji, Z. Lin, M. Alcoutlabi and X. Zhang, *Energy Environ. Sci.*, 2011, **4**(8), 2682.

2 F.-W. Yuan, H.-J. Yang and H.-Y. Tuan, *ACS Nano*, 2012, **6**(11), 9932–9942.

3 J.-G. Ren, Q.-H. Wu, H. Tang, G. Hong, W. Zhang and S.-T. Lee, *J. Mater. Chem. A*, 2013, **1**(5), 1821.

4 L. Baggetto and P. H. L. Notten, *J. Electrochem. Soc.*, 2009, **156**(3), A169–A175.

5 Y. Yu, L. Gu, C. Wang, A. Dhanabalan, P. A. van Aken and J. Maier, *Angew. Chem.*, 2009, **48**(35), 6485–6489.

6 L. P. Tan, Z. Lu, H. T. Tan, J. Zhu, X. Rui, Q. Yan and H. H. Hng, *J. Power Sources*, 2012, **206**, 253–258.

7 K. T. Lee, J. C. Lytle, N. S. Ergang, S. M. Oh and A. Stein, *Adv. Funct. Mater.*, 2005, **15**(4), 547–556.

8 Y. Hwa, C.-M. Park, S. Yoon and H.-J. Sohn, *Electrochim. Acta*, 2010, **55**(9), 3324–3329.

9 T. Song, Y. Jeon, M. Samal, H. Han, H. Park, J. Ha, D. K. Yi, J.-M. Choi, H. Chang, Y.-M. Choi and U. Paik, *Energy Environ. Sci.*, 2012, **5**(10), 9028.

10 M. G. Kim and J. Cho, *J. Electrochem. Soc.*, 2009, **156**(4), A277–A282.

11 J. Graetz, C. C. Ahn, R. Yazami and B. Fultz, *Electrochem. Solid-State Lett.*, 2003, **6**(9), A194–A197.

12 G. Cui, L. Gu, L. Zhi, N. Kaskhedikar, P. A. van Aken, K. Müllen and J. Maier, *Adv. Mater.*, 2008, **20**(16), 3079–3083.

13 S. Yoon, C.-M. Park and H.-J. Sohn, *Electrochem. Solid-State Lett.*, 2008, **11**(4), A42.

14 D. J. Xue, S. Xin, Y. Yan, K. C. Jiang, Y. X. Yin, Y. G. Guo and L. J. Wan, *J. Am. Chem. Soc.*, 2012, **134**(5), 2512–2515.

15 C. K. Chan, X. F. Zhang and Y. Cui, *Nano Lett.*, 2008, **8**(1), 307–309.

16 M. H. Park, Y. Cho, K. Kim, J. Kim, M. Liu and J. Cho, *Angew. Chem.*, 2011, **50**(41), 9647–9650.

17 M. H. Park, K. Kim, J. Kim and J. Cho, *Adv. Mater.*, 2010, **22**(3), 415–418.

18 M.-H. Seo, M. Park, K. T. Lee, K. Kim, J. Kim and J. Cho, *Energy Environ. Sci.*, 2011, **4**(2), 425.

19 H. Lee, M. G. Kim, C. H. Choi, S. Yang-Kook, C. S. Yoon and J. Cho, *J. Phys. Chem. B*, 2005, **109**(44), 20719–20723.

20 C.-M. Park and H.-J. Sohn, *J. Chem. Eng. Mater. Sci.*, 2008, **20**(9), 3169–3173.

21 J. Graetz, C. C. Ahn, R. Yazami and B. Fultz, *Electrochem. Solid-State Lett.*, 2003, **6**(9), A194.

22 I. Sandu, P. Moreau, D. Guyomard, T. Brousse and L. Roue, *Solid State Ionics*, 2007, **178**(21–22), 1297–1303.

23 M. N. Obrovac, L. Christensen, D. B. Le and J. R. Dahn, *J. Electrochem. Soc.*, 2007, **154**(9), A849.

24 J.-H. Kim, H. Kim and H.-J. Sohn, *Electrochem. Commun.*, 2005, **7**(5), 557–561.

25 J. Saint, M. Morcrette, D. Larcher, L. Laffont, S. Beattie, J. P. Pérès, D. Talaga, M. Couzi and J. M. Tarascon, *Adv. Funct. Mater.*, 2007, **17**(11), 1765–1774.

26 G. Cui, L. Gu, L. Zhi, N. Kaskhedikar, P. A. van Aken, K. Müllen and J. Maier, *Adv. Mater.*, 2008, **20**(16), 3079–3083.

27 I.-S. Hwang, J.-C. Kim, S.-D. Seo, S. Lee, J.-H. Lee and D.-W. Kim, *Chem. Commun.*, 2012, **48**(56), 7061–7063.

28 K. H. Seng, M. H. Park, Z. P. Guo, H. K. Liu and J. Cho, *Angew. Chem., Int. Ed.*, 2012, **51**(23), 5657–5661.

29 Z. H. Bao, M. R. Weatherspoon, S. Shian, Y. Cai, P. D. Graham, S. M. Allan, G. Ahmad, M. B. Dickerson, B. C. Church, Z. T. Kang, H. W. Abernathy, C. J. Summers, M. L. Liu and K. H. Sandhage, *Nature*, 2007, **446**(7132), 172–175.

30 Y. Yu, L. Gu, C. Zhu, S. Tsukimoto, P. A. van Aken and J. Maier, *Adv. Mater.*, 2010, **22**(20), 2247.

31 H. Kim, M. Seo, M.-H. Park and J. Cho, *Angew. Chem., Int. Ed.*, 2010, **49**(12), 2146–2149.

32 Y. Yu, C. Yan, L. Gu, X. Lang, K. Tang, L. Zhang, Y. Hou, Z. Wang, M. W. Chen, O. G. Schmidt and J. Maier, *Adv. Energy Mater.*, 2013, **3**(3), 281–285.

33 L. C. Yang, Q. S. Gao, L. Li, Y. Tang and Y. P. Wu, *Electrochem. Commun.*, 2010, **12**(3), 418–421.

34 Y.-X. Yin, S. Xin, L.-J. Wan, C.-J. Li and Y.-G. Guo, *J. Phys. Chem. C*, 2011, **115**(29), 14148–14154.

35 J.-Y. Shin, D. Samuelis and J. Maier, *Adv. Funct. Mater.*, 2011, **21**, 3464–3472.